Original Research

Monitoring the Variation in Driver Respiration Rate from Wakefulness to Drowsiness: A Non-Intrusive Method for Drowsiness Detection Using Thermal Imaging

Serajeddin Ebrahimian Hadi Kiashari[1]*, Ali Nahvi[1], Amirhossein Homayounfard[1], Hamidreza Bakhoda[1]

[1.] *Department of Mechatronics Engineering, School of Mechanical Engineering, K. N. Toosi University of Technology, Tehran, Iran*

Received: 07 Mar. 2018 Accepted: 24 May. 2018

Abstract

Background and Objective: Driver drowsiness is a cause of many traffic accidents all around the world. Driver respiration dynamics undergoes significant changes from wakefulness to sleep. The intrusive nature of current respiration monitoring methods makes them unattractive for detection of in-vehicle driver drowsiness. In this paper, changes in the respiration rate were monitored for drowsiness detection using thermal imaging, which is completely contact-free and non-intrusive.

Materials and Methods: For each frame, the driver's face was isolated from the rest of the image. Then, the nostrils' zone was localized using physiological characteristics of face. The respiration signal was constructed by putting together the mean temperature of nostril region in all of the frames. In order to study respiration variations from wakefulness to drowsiness, a total number of 12 subjects were tested in a driving simulator. The observer rating of drowsiness (ORD) method was used to estimate the drowsiness level of the subjects.

Results: Derivation of driver respiration rate using thermal imaging was a reliable and non-intrusive method. The results were strongly correlated with those of traditional methods. Driver respiration rate decreased from wakefulness to extreme drowsiness by 3.5 breaths per minute (bpm) and its standard deviation (SD) increased by 0.7 bpm.

Conclusion: Driver respiration rate decreased and its SD increased from wakefulness to drowsiness in 12 participants of this study. The results showed that driver drowsiness could be detected even at moderate levels from analysis of the respiration rate.

Keywords: Sleep; Respiration; Automobile driving; Thermography

Citation: Ebrahimian-Hadikiashari S, Nahvi A, Homayounfard A, Bakhoda H. **Monitoring the Variation in Driver Respiration Rate from Wakefulness to Drowsiness: A Non-Intrusive Method for Drowsiness Detection Using Thermal Imaging.** J Sleep Sci 2018; 3(1-2): 1-9.

Introduction

Driver drowsiness is one of the main causes of traffic accidents all over the world. Detection systems for driver drowsiness can be effective in reducing such accidents (1). Driver drowsiness may occur as a result of sleep deprivation, long working hours, and sleep disorders. Sleep disorders can have a high impact on the quality of sleep and consequently the performance of the driver (2). People suffering from a sleep disorder, like apnea, are normally sleepy during the day and have poor sleep quality, which makes them more susceptible to accidents (3, 4).

The human respiratory system undergoes noticeable changes from wakefulness to sleep. Various features of the human respiratory system change during this transition and can be regarded as indicators of drowsiness. The respiration rate and the inspiration-to-expiration ratio (I:E ratio) are among the most notable ones. Several studies have measured and analyzed changes of these parameters during sleep and wakefulness (5, 6).

**** Corresponding author**: S. Ebrahimian-Hadikiashari, Department of Mechatronics Engineering, School of Mechanical Engineering, Khajeh Nasir Toosi University of Technology, Tehran, Iran*
Tel: +98 9365766384, Fax: +98 21 88674748
Email: sebrahimian@mail.kntu.ac.ir

However, a few researches considered these changes while the person was drowsy. For instance, one of the studies analyzed the respiratory effort during transition from wakefulness to drowsiness (7).

Thermal imaging is a desirable tool for extracting human vital signs by measuring temperature changes of the skin. Over the past decade, infrared thermal imaging has been used in various areas of research including medicine, biometrics, and machine vision (8). This method only uses the radiation emitted naturally from the human body and does not require contact with the body or aiming any kind of radiation at the body (9). Because of being contact-free and non-intrusive, this method has been widely used in studies related to the human body (10). Recent research works have shown that respiratory states of a person can be monitored without interference using thermal imaging. The data extracted by thermal imaging is highly correlated with those extracted by other methods (11). Monitoring respiration using thermal imaging is achieved by observing the difference in temperature between the environment and the air exiting the respiration system. As this method does not interfere with the person's activity, it is also ideal for use in applications related to cognition and emotion assessment.

This paper presents the results of the first research that analyzed driver's respiration variations from wakefulness to micro-sleeps using thermal imaging. The mean and standard deviation (SD) of the respiration rate were studied in 2-minutes intervals in various states of drowsiness. The observer rating of drowsiness (ORD) (12) was used to estimate different levels of drowsiness. To evaluate this method, 12 subjects were tested in a driving simulator.

Materials and Methods

To study variations of respiration rate from wakefulness to drowsiness, driving tests were performed in a driving simulator. A thermal camera and a night vision camera were used to monitor the driver. The tests were conducted on an endless highway according to an experimental protocol to provide all stages of drowsiness for the subjects. The ORD method was used to estimate drowsiness levels.

Signal extraction: To extract the respiration signal, the video recorded by the camera was converted into a sequence of frames. Then, the subject's face was extracted from the image. The target zone (the nostrils) was detected using characteristics of facial temperature. The mean of the intensity of the pixels -temperature- in this zone was extracted for each frame. Finally, the respiration signal was constructed by putting together the intensity values for all frames.

- ***Face extraction:*** Face detection and separation from the background was the first step to extract the subject's respiration signal. To accomplish this extraction, the algorithm presented by Bakhoda (13) was used. This method utilizes a thresholding method to separate the image of the person from the background as shown in figure 1.

Figure 1. Original image (a); the image after thresholding (b)

Next, the horizontal and vertical signatures of the binary image were used to separate the face from the rest of the body. As shown in figure 2 (a), most white pixels were concentrated at the driver's face. Figures 2 (b) and (c) show the number of white pixels in each row and column of the image. The face region can be extracted at the neighborhood of the maximum horizontal and vertical signatures of the binary image as shown in figure 2 (d).

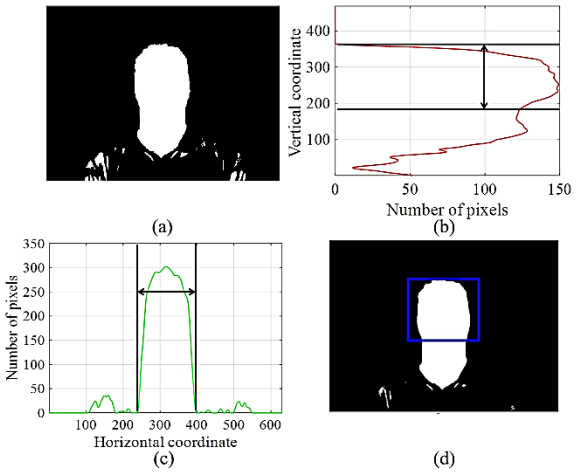

Figure 2. Face localization: binary image (a), horizontal component of the binary image (b), vertical component of the binary image (c), and face localization in the binary image (d)

Finally, after using this method, the image of the face can be easily extracted in the same area as the binary image, as shown in figure 3.

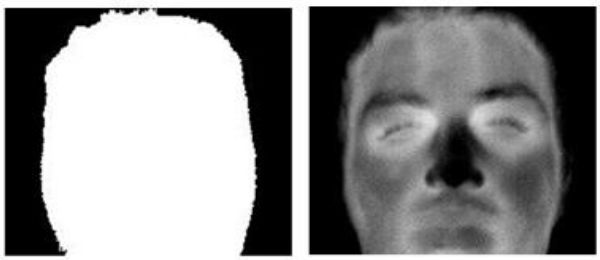

Figure 3. Threshold of the face (a), the final image of the face (b)

- ***Respiration region extraction:*** After extracting the face from the background, the respiration region needs to be extracted. We should locate part of the image that experiences oscillatory changes during respiration. The respiration signal can then be extracted by constant monitoring of this zone, which is located below the nostrils. Detection of this zone is the most important part of respiration signal extraction. Therefore, special attention has to be paid to utilize a method that is simple, fast, and as free of errors as possible. Previously, in studies conducted by Zhu (14) and Pereira et al. (15), various methods were presented to extract the target zone and track it throughout the subsequent frames. In the method employed by Zhu (14), facial key points were first set manually and then tracked using tracking algorithms. A more suitable method of thresholding was presented by Pereira et al. (15). In this method, the image of the person's face was divided into equal areas. Afterwards, the middle area of the face was selected as a potential region for respiration extraction. Then using edge detection algorithms and morphological shape of the nose, the region related to respiration was extracted.

In this paper, we used facial temperature distribution to locate the target area robustly. The periorbital region – the area between the inner corner of an eye and the nose – often has the highest temperature of the face because of the high number of capillaries. In addition, the lower part of the subject's nose has the lowest temperature since it has a small number of capillaries with a large heat-dissipating surface area. However, facial temperature distribution is not the same for all people. For instance, the area surrounding the temporal artery may have a higher temperature than the periorbital region. Additionally, the hair temperature is equal to that of the surroundings and lower than the nose, as there is no blood flow within the hair. These two facts can lead to unexpected errors in finding the target zone. For that reason, we performed the search in a more limited area instead of the full face. This area was the central region of the face, which could be easily determined by partitioning the image into equal areas. The search region is shown by a green rectangle in figure 4.

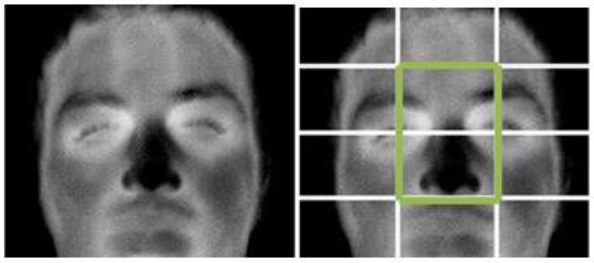

Figure 4. Original image (a), partitioned image and the green search region (b)

The target zone could be extracted from the search region. Since the search is only performed in the central region, it can be robustly assumed that the area with the highest temperature corresponds to the periorbital region and the one with the lowest temperature is the nose. Therefore, the two pixels that represent center of two hot-temperature regions and are not close to each other were selected as the corners of the eyes. A line segment was drawn by connecting these two pixels. The pixel located on the perpendicular bisector of this line segment that had the lowest temperature was selected as the tip of the nose. The area directly below the tip of the nose was the respiration target zone (Figure 5).

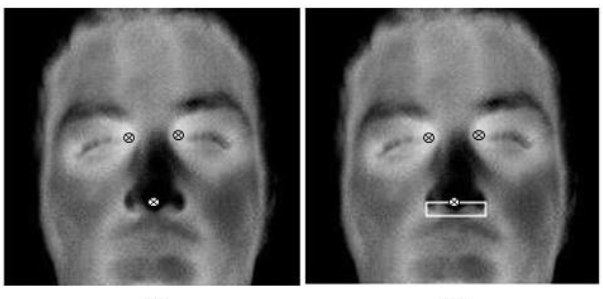

Figure 5. Points corresponding to the corners of the eyes and the tip of the nose (a), target zone (b)

The respiration signal was constructed by taking the average temperature of pixels within the target zone for each frame. A subject was asked to breathe according to a certain pattern: breathe normally, take a deep breath, breathe normally, breathe rapidly, and breathe normally again. As shown in figure 6, the subject took a normal breath for 18 seconds, a deep breath from t = 18s to t = 24s, again a normal breath from t = 24s to t = 31s, a rapid breath from t = 31s to t = 42s, and again a normal breath from t = 42s to t = 59s. As shown in figure 6, the temperature within the target zone distinguishes deep breathing and rapid breathing from normal breathing.

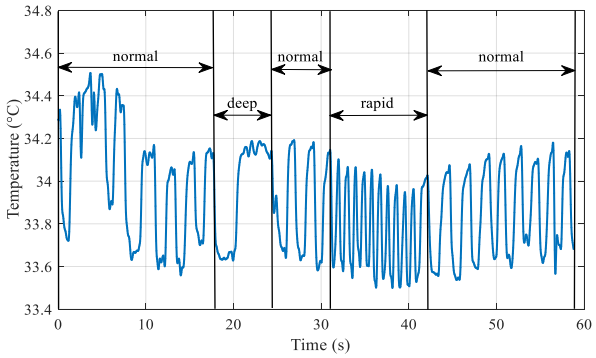

Figure 6. Respiration signal extracted from thermal images

- ***Post-processing and noise reduction:*** Since small errors can occur in the detection of the target zone and taking the average of the pixels, it is necessary to perform a noise reduction process on the signal. For this purpose, an infinite impulse response (IIR) Butterworth low-pass filter with a cutoff frequency of 0.6 Hz was designed. The filter removes all high-frequency noises without changing the overall shape of the signal for feature extraction purposes.

Feature extraction: The extracted respiration signal $\mathrm{Resp}(t)$ can be modeled using this equation:

$$\mathrm{Resp}(t) = A(t).S\big(\theta(t)\big) + W(t) \qquad (1)$$

Where $A(t)$ is the signal amplitude function, S is the form of the respiration signal – a combination of sine and cosine functions, $\theta(t)$ is the phase function whose derivative equals the instantaneous frequency of the signal – the breathing rate, and $W(t)$ includes other signal forms like high-frequency noises and the varying baseline values of the signal.

The main features of the signal were $A(t)$, $\theta(t)$, and $W(t)$ according to Eq. 1. Occasional deviation of the target zone from the respiration region during the extraction process and temporal changes in the environmental temperatures may cause relatively large changes in the respiration signal extracted from thermal images. Such anomalies make $A(t)$ and $W(t)$ less useful. Hence, $\theta(t)$ and its derivative - the respiration frequency - are the most reliable features that should be analyzed.

Time-frequency analysis is a suitable method to analyze respiration signal because of its non-stationary nature. Synchrosqueezed wavelet transform presents time-frequency components of the signal (16). It aims to improve the time-frequency display of a signal by giving its value to another point in the same time-frequency space by analyzing the local behavior of the signal around that point.

Figure 7 shows the filtered respiration signal and the instantaneous breathing rate extracted by the synchrosqueezed wavelet transform. Figure 7 (a) shows both the original and the filtered respiration signal. The filter removes sharp corners of the original signal while preserving the overall shape and the low-frequency content of the signal. As shown in figure 7 (b), the subject's breathing rate is in accordance with the breathing pattern described before.

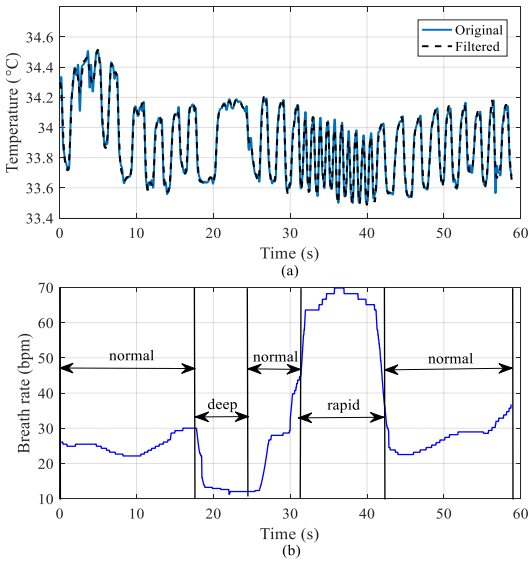

Figure 7. Respiration signal (a), derived breathing rate (b)

The breathing rate was initially at 25 breaths per minute (bpm) and remained relatively constant. Then, it decreased to 12 bpm from t = 18s to t = 24s, as the subject took a deep breath. The breathing rate returned back to normal for 7

seconds as the subject took a normal breath again from t = 24s to t = 31s. A significant increase to 65 bpm occurred due to rapid breathing from t = 31s to t = 42s. Finally, the breathing rate returned back to normal and lasted till t = 59s.

This thermal imagining method was verified with breathing rates calculated by human observers. Five healthy subjects with a regular sleep pattern were selected and participated in a 5-minute test. The tests were divided into five 1-minute intervals. The reference breathing rate was estimated by two trained human observers who counted the number of breaths in the 1-minute intervals. The Bland-Altman plot and the linear correlation analysis were used to evaluate the accuracy of the methods. Figure 8 shows correlation analysis and Bland-Altman plot of the reference breathing rate (BR_{ref}) and the breathing rate of thermal imaging method (BR_{ti}).

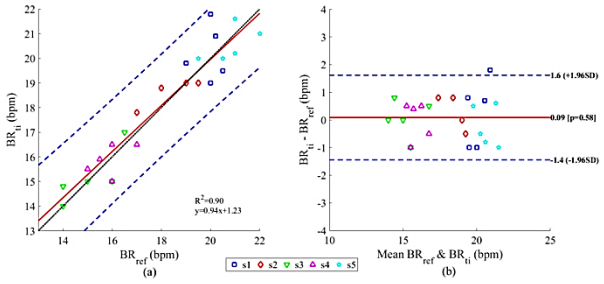

Figure 8. Correlation between the reference breathing rate (BR_{ref}) and the thermal imaging breathing rate (BR_{ti}). The solid red line is the fitted curve, the black line is perfect match line, and the blue dashed lines are 95% limits of agreement (a), the Bland-Altman plot of the difference against average breathing rate of the two methods. SD is the standard deviation. The solid red line indicates the mean difference and dashed blue lines indicate 95% limits of agreement (b).

As shown in figure 8 (a), the breathing rate estimated by thermal imaging was strongly correlated with the reference method. All scatter points were within 95% agreement lines and the regression line was close to the line of a perfect match. The Bland-Altman plot of the thermal imaging method and the reference method was shown in figure 8 (b). As shown in figure 8 (b), there was a mean difference of 0.09 bpm and the limits of agreement were -1.4 and 1.6 bpm. Only one measurement point exceeds 95% lines of agreement due to abnormal head movement of the subject.

Driving simulator: Experiments were conducted in a driving simulator. The driving simulator was built at the virtual reality laboratory of Khajeh Nasir Toosi University of Technology from one-quarter body of a full sedan. The steering wheel torque feedback simulating road lateral force was applied by a 700-W AC servo motor. The display consisted of three wide monitors as shown in figure 9.

Figure 9. Side view of the driving simulator

Data acquisition tools: A thermal camera was used to capture temperature profile and extract the respiration rate (Figure 10). A night vision camera was installed in front of the driver to monitor and capture the subject's face. This video from the night vision camera was later used to determine the drowsiness level of the drivers using the ORD method. Temperature and humidity of the environment were recorded by five sensors with a sampling rate of 0.2 *Hz* during the tests. The data showed that humidity and temperature variations were negligible during the experiments with the mean SD of 0.16% and 0.17 *°C*, respectively.

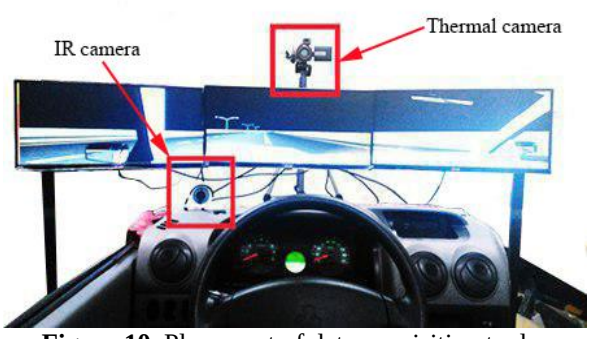

Figure 10. Placement of data acquisition tools

Study participants: Fifteen subjects participated in the experiments. The subjects aged between 23 and 29 with the average body mass index (BMI) of 25. They possessed driver's license, had on average 3 years of driving experience, and drove at least about 8 hours a week. The driving tests were performed between 10 pm to 6 am in a dark room. Figure 11 shows thermal images of the participants.

Figure 11. Thermal images of the subjects

Three subjects were excluded from the study, two of them had eyeglasses. Eyeglasses alter the thermal pattern captured by the thermal camera, as infrared radiation does not pass through the glass. One of these three subjects was an athlete with a history of abuse of performance enhancement substances. Therefore, the data of 12 out of 15 subjects were analyzed in this paper.

Before the start of the test, each driver had a 15-minute drill session to get familiar with the driving simulator. This drill session also helped reduce subjects' stress and excitement. All subjects were asked to reduce their sleeping time down to 4 hours a day in the last three days leading to the test night and not to eat or drink stimulant substances for 24 hours before the test. No participant had a history of respiratory or sleep disorders.

The subjects signed a consent form to fully observe the experimental protocol. The study protocol was approved by Khajeh Nasir Toosi University of Technology in accordance with the Declaration of Helsinki.

Driving scenario: Subjects were required to drive on a quasi-circular loop. The path was a three-lane highway with a shoulder on the right and a guardrail on the left. If the driver fell asleep, the vehicle would go off the road or bump into the guardrail. The road map is shown in figure 12. No traffic or obstacle existed on the road to prevent driver distraction. The environment represented a boring desert in twilight.

The drivers were asked to try to keep a constant speed of 80 km/hour. They were required to stay on the middle lane; so that, they would have enough time to react if the vehicle departed off the lane. If the car departed off the road or collided with the guardrail, the test would end. Each test lasted at most 2 hours.

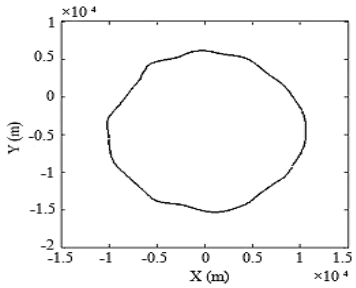

Figure 12. The quasi-circular loop of the three-lane highway

Validation: To validate the drowsiness level of the drivers, the ORD method was employed (12). In this method, the face and the behavior of the driver were monitored by three people of the research team during the driving process. Each observer rated the driver's drowsiness using a number from 1 to 5 based on changes in certain facial and behavioral features. A score of 1 represents no drowsiness and a score of 5 represents extreme drowsiness.

Results

The respiration signal of each driver was extracted using the thermal videos captured during the tests. The demographic characteristics of the subjects and the environmental data of the test room are shown in table 1.

Table 1. Demographic characteristics of the subjects and the environment's data

Subject number	Age (year)	Height (m)	Weight (kg)	BMI (kg/m^2)	Room humidity % (SD)	Room temperature (℃) (SD)
1	25	1.79	80	24.96	46.15 (0.34)	23.78 (0.17)
2	23	1.83	88	26.27	44.67 (0.25)	24.29 (0.32)
3	24	1.81	75	22.89	45.36 (0.06)	24.30 (0.40)
4	25	1.86	80	23.12	47.35 (0.12)	24.37 (0.08)
5	25	1.75	75	24.48	41.82 (0.12)	23.51 (0.16)
6	25	1.73	83	27.73	43.25 (0.09)	23.68 (0.03)
7	26	1.71	85	29.06	44.12 (0.23)	22.86 (0.11)
8	22	1.70	68	23.52	46.62 (0.11)	23.12 (0.30)
9	28	1.88	80	22.63	43.61 (0.09)	22.70 (0.33)
10	25	1.82	90	27.17	45.74 (0.20)	22.80 (0.30)
11	27	1.72	80	27.04	43.15 (0.13)	22.08 (0.08)
12	25	1.89	100	27.99	44.95 (0.25)	23.28 (0.12)
Mean	25	1.79	82	25.57	44.73 (0.16)	23.40 (0.17)

BMI: Body mass index; SD: Standard deviation

Figure 13 shows the respiration signal, the drowsiness level using the ORD method, and the respiration rate for one of the 12 subjects.

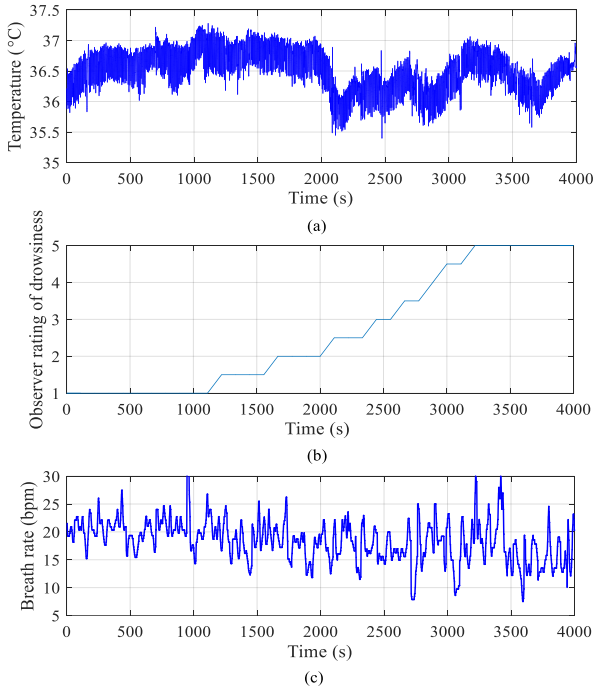

Figure 13. Respiration signal extracted from the driving scenario (a), observer rating of drowsiness (ORD) (b), instantaneous respiration rate (c)

As shown in figure 13 (c), as drowsiness level increased from 1 to 5, the breathing rate mean decreased from 20 bpm to 16 bpm. The respiration rate signal had two major drops for this subject. One major decline occurred at moderate drowsiness (ORD = 3) and another major decline at extreme drowsiness (ORD = 5). In figure 13 (c), the amplitude of oscillation increased at higher levels of drowsiness; there was a higher SD of the respiration rate at ORD = 4 and ORD = 5.

The breathing rate was analyzed as the drivers experienced different stages of drowsiness. Three groups of 2-minute intervals corresponding to three levels of drowsiness – not drowsy (ORD = 1), moderately drowsy (ORD = 3), and extremely drowsy (ORD = 5) – were considered. The mean and the SD of the respiration rate of the drivers were obtained as shown in figures 14 and 15.

As shown in figure 14, the mean respiration rate of the subjects decreased as the subject's drowsiness level increased. The median of the mean of the respiration rate was initially at 19 bpm. At the moderate level of drowsiness, it decreased by about 1.5 bpm, and decreased by another 2.0 bpm at extreme drowsiness reaching to 3.5 bpm.

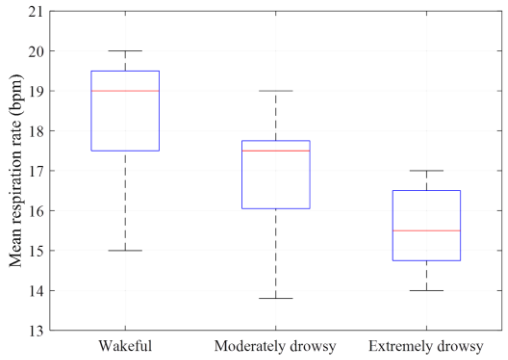

Figure 14. Box plot showing the mean of the respiration rate in 2-minute time intervals from wakefulness to extreme drowsiness

Therefore, respiration rate can be used as a leading indicator of drowsiness allowing for appropriate measures to be taken approximately 15 minutes before a drowsiness-related accident.

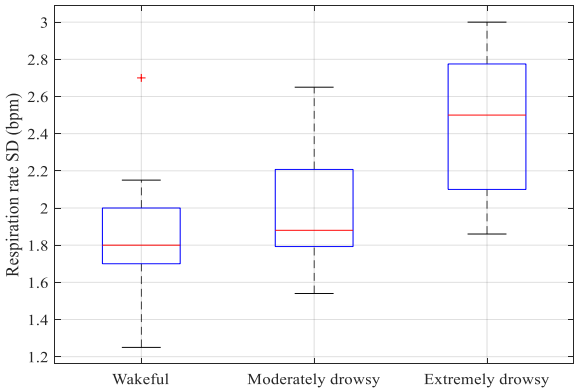

Figure 15. Box plot showing the standard deviation (SD) of the respiration rate from wakefulness to extreme drowsiness

As shown in figure 15, the SD of the respiration rate increased as the subject's drowsiness level increased. The median of the SD of the respiration rate was initially at 1.80 bpm. At the moderate level of drowsiness, it increased by about 0.08 bpm, and increased by another 0.62 bpm at extreme drowsiness reaching to 0.70 bpm. The relatively small change of SD from wakefulness to moderate drowsiness is because some subjects experienced decrements rather than increments. The SD of respiration rate is complementary for detecting drowsiness at the moderate drowsiness level and should not be used alone for this moderate stage. However, the SD of the respiration rate

had a notable increase of 33% in transition from moderate drowsiness to extreme drowsiness. In figure 14, the decrease in the mean respiration rate was only 11.5% in transition from moderate drowsiness to extreme drowsiness. Thus, the SD in figure 15 is a strong indicator of extreme drowsiness, even though it is not as early as the mean respiration rate.

Discussion

In this study, respiration rate of drivers was analyzed non-intrusively using thermal imaging. Since most respiration measurement methods need contact with the body, few researches have been conducted on drivers' respiration for detecting drowsiness. In this paper, the thermal video was converted into a sequence of images. The subject's face was localized and extracted from the image. Finally, the respiration signal was constructed by bundling the average temperature of the nostrils area for all frames. The mean and the SD of the respiration rate were extracted from the respiration signal in two-minute intervals. The breathing rate estimated by thermal imaging was strongly correlated with a reference method. All scatter points were within 95% agreement lines.

A thermal camera was placed in front of the driver in a driving simulator to study variations of driver's respiration rate from wakefulness to drowsiness. The respiration rates of 12 drivers were extracted in different stages of drowsiness. The ORD method was used to score the drowsiness level of driver. The results showed that the respiration rate of the subjects decreased by 1.5 bpm from wakefulness to moderate drowsiness and another 2.0 bpm from moderate drowsiness to extreme drowsiness. The SD of the respiration rate from wakefulness to moderate drowsiness increased by only 0.08 bpm, but experienced a substantial increase of 0.62 bpm from moderate drowsiness to extreme drowsiness. According to the results, driver's drowsiness can be detected from the respiration signal long before it reaches extreme drowsiness.

In this research, three drowsiness states were studied. Some other researches studied only two states of drowsiness (7). The results obtained by Rodríguez-Ibáñez et al. shows a decrease of 4.20 bpm in the mean respiration rate and an increase of 1.62 bpm in the SD of respiration rate from wakefulness to drowsiness. Corresponding values obtained in our research were a decrease of 3.50 bpm in the mean respiration rate and an increase of 0.70 bpm in the SD of respiration rate from wakefulness to extreme drowsiness (7).

Spatio-temporal algorithms are more robust compared to spatial algorithms. The regional restriction method used in this paper was designed as simple as possible, and the region extraction method was iterated for each frame. A region tracker could be used to reduce computational cost. Conditions altering the regular facial temperature pattern would not affect performance of spatio-temporal algorithms. For example, such algorithms will remain robust even if the driver wears eyeglasses or suffers a temperature-altering illness. The algorithm presented in this paper can be further improved by applying supervised classifiers such as k-nearest neighbors (KNN) (17) and support vector machine (SVM) (17).

The contact-free method used in this paper can also be used in future studies to detect distraction, analyze health status, or identify various illnesses. In future studies, respiration change for people with sleep disorders – narcolepsy and apnea – can be also analyzed.

Conclusion

Monitoring driver's respiration through thermal imaging is reliable and non-intrusive. Based on the data obtained from 12 subjects, driver respiration rate decreases and its SD increases from wakefulness to drowsiness. The results indicate that drivers' drowsiness can be detected even at moderate levels of drowsiness providing enough lead time for potential intervention.

Conflict of Interests

Authors have no conflict of interests.

Acknowledgments

This paper is based upon a work supported by the Cognitive Science and Technology Council (CSTC) under Grant No. 1307.

References

1. Sigari MH, Fathy M, Soryani M. A driver face monitoring system for fatigue and distraction detection. International Journal of Vehicular Technology 2013; 2013: 263983.

2. Joorabbaf MS, Shabany M, Sadeghniiat HK, et al. Relationship between sleep quality, obstructive sleep apnea and sleepiness during day with related fac-

tors in professional drivers. Acta Med Iran 2017; 55: 690-5.

3. Dinges DF. An overview of sleepiness and accidents. J Sleep Res 1995; 4: 4-14.

4. Stoohs RA, Guilleminault C, Dement WC. Sleep apnea and hypertension in commercial truck drivers. Sleep 1993; 16: S11-S13.

5. Trinder J, Whitworth F, Kay A, et al. Respiratory instability during sleep onset. J Appl Physiol (1985) 1992; 73: 2462-9.

6. Douglas NJ, White DP, Pickett CK, et al. Respiration during sleep in normal man. Thorax 1982; 37: 840-4.

7. Rodríguez-Ibáñez N, García González MÁ, Fernández Chimeno M, et al. Synchrosqueezing index for detecting drowsiness based on the respiratory effort signal. Proceedings of the 13th Mediterranean Conference on Medical and Biological Engineering and Computing; 2013 Sep. 25-28; Seville, Spain; 2013. p. 965-8.

8. Gade R, Moeslund TB. Thermal cameras and applications: A survey. Mach Vis Appl 2014; 25: 245-62.

9. Gustavsson R. Termography: A practical approach. Olofstrom, Sweden: Norbo kraftteknik AB; 2009.

10. Ring EF, Ammer K. Infrared thermal imaging in medicine. Physiol Meas 2012; 33: R33-R46.

11. Pereira CB, Yu X, Czaplik M, et al. Remote monitoring of breathing dynamics using infrared thermography. Biomed Opt Express 2015; 6: 4378-94.

12. Wierwille WW, Ellsworth LA. Evaluation of driver drowsiness by trained raters. Accid Anal Prev 1994; 26: 571-81.

13. Bakhoda H. Analysis and implementation of a new driver drowsiness detection system based on thermal infrared imaging of the face [Thesis]. Tehran, Iran: K. N. Toosi University of Technology; 2015. [In Persian].

14. Zhu Z. Tracking human breath in infrared imaging. Proceedings of the 5th IEEE Symposium on Bioinformatics and Bioengineering; 2005 Oct. 19-21: Minneapolis, MN; 2005. p. 227-31.

15. Pereira CB, Yu X, Blazek V, et al. Robust remote monitoring of breathing function by using infrared thermography. Conf Proc IEEE Eng Med Biol Soc 2015; 2015: 4250-3.

16. Daubechies I, Lu J, Wu HT. Synchrosqueezed wavelet transforms: An empirical mode decomposition-like tool. Appl Comput Harmon Anal 2011; 30: 243-61.

17. Kotsiantis SB. Supervised machine learning: A review of classification techniques. Informatica 2007; 31: 249-68.